Energetics of the Human Tel-22 Quadruplex−Telomestatin Interaction: A Molecular Dynamics Study

Saurabh Agrawal,[†] Rajendra Prasad Ojha,*[,‡] and Souvik Maiti*[,†]

Proteomics and Structural Biology Unit, Institute of Genomics and Integrative Biology, CSIR, Mall Road, New Delhi 110007, India, and Biophysics Unit, Department of Physics, DDU Gorakhpur University, Gorakhpur 273009, India

Received: October 24, 2007; Revised Manuscript Received: February 20, 2008

The formation and stabilization of telomeric quadruplexes has been shown to inhibit the activity of telomerase, thus establishing telomeric DNA quadruplex as an attractive target for cancer therapeutic intervention. In this context, telomestatin, a G-quadruplex-specific ligand known to bind and stabilize G-quadruplex, is of great interest. Knowledge of the three-dimensional structure of telomeric quadruplex and its complex with telomestatin in solution is a prerequisite for structure-based rational drug design. Here, we report the relative stabilities of human telomeric quadruplex ($AG_3[T_2AG_3]_3$) structures under K^+ ion conditions and their binding interaction with telomestatin, as determined by molecular dynamics simulations followed by energy calculations. The energetics study shows that, in the presence of K^+ ions, mixed hybrid-type Tel-22 quadruplex conformations are more stable than other conformations. The binding free energy for quadruplex−telomestatin interactions suggests that 1:2 binding is favored over 1:1 binding. To further substantiate our results, we also calculated the change in solvent-accessible surface area (ΔSASA) and heat capacity (ΔC_p) associated with 1:1 and 1:2 binding modes. The extensive investigation performed for quadruplex−telomestatin interaction will assist in understanding the parameters influencing the quadruplex−ligand interaction and will serve as a platform for rational drug design.

Introduction

Telomeres are specialized nucleoprotein complexes at eukaryotic chromosomal termini. They comprise of 4–14 kb-DNA sequences with a 50–200-nucleotide 3′ single-stranded overhang consisting of GT-rich 6-nucleotide tandem repeats (5′-TTAGGG-3′/3′-AATCCC-5′) in humans.[1–3] Telomeric DNA and associated proteins have essential roles in protection of chromosomal ends from fusion, recombination, and exonucleolytic degradation.[4] The inability of polymerase enzymes to extend single-stranded DNA leaves 50–200 bases of the telomeric overhang unreplicated in each cell cycle, leading to the continuous shortening of chromosomal ends and ultimately culminating in replicative senescence.[5] However, cancerous cells escape senescence by activating an enzyme called telomerase, a ribonucleoprotein that interacts with the telomeric 3′ overhang via its 11-nucleotide RNA template to allow addition of tandem repeats so as to keep telomeric ends unaffected.[6] G-rich tandem repeats at telomeric ends have been shown to form an unusual four-stranded quadruplex structure, assembled by Hoogsteen hydrogen bonding between the guanines and stabilized by cations in the center of the quartets (especially K^+ ions).[7,8] The stabilization of the telomeric quadruplex with assistance from small molecules[9] inhibits the hybridization of the RNA template of telomerase with single-stranded telomeric DNA, thus inhibiting telomere elongation by telomerase enzyme.[6] Therefore, telomerase inhibition through stabilization of the quadruplex has shown great promise for selective cancer therapeutics.[10–12] A number of quadruplex binders such as anthraquinones,[13–15] perylenes,[16–18] quinolones,[19] porphyrines,[20–23] and oxazoles[24] have been proposed as potential drug candidates.

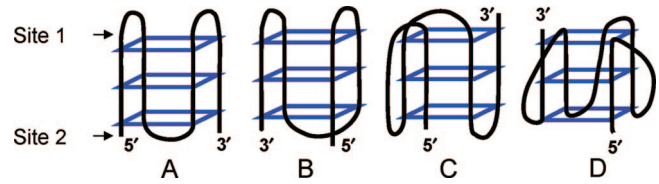

Figure 1. Schematic representation of human Tel-22 quadruplex conformations: (A) antiparallel basket-type, (B) antiparallel chair-type, (C) mixed hybrid-type, and (D) parallel propeller-type. Sites 1 and 2 are the two telomestatin binding sites.

The intramolecular human telomeric quadruplex can attain antiparallel basket-type, antiparallel chair-type, parallel propeller-type, and mixed hybrid-type conformations (Figure 1) depending on the nucleotide length and ionic conditions.[25–28] Literature studies based on NMR data reveal that the Tel-22 sequence forms a well-defined basket-type intramolecular G-quadruplex in the presence of Na^+ ions.[25] Using the platinum cross-linking method,[29] Redon et al. showed that the antiparallel basket-type conformation forms in the presence of both Na^+ and K^+ ions. Another report based on the ^{25}I-radioprobing technique supported the formation of the antiparallel chair-type conformation in the presence of K^+ ions and the antiparallel basket-type conformation in the presence of Na^+ ions.[28] Shafer and co-workers also found the antiparallel chair-type conformation to be present under K^+ ion conditions with the chemical ligation method.[30] An X-ray crystal study of Tel-22 found the parallel propeller-type conformation in the presence of K^+ ions.[26] Another report based on simulations showed that Tel-22 adopts the chair-type conformation in the presence of K^+

* Phone +91-11-27666156(S.M.), +91-551-2202167(R.P.O.). Fax: +91-11-27667471 (S.M.), +91-551-2340459 (R.P.O.). E-mail: souvik@igib.res.in (S.M.), rp_ojha@yahoo.com (R.P.O.).
† Institute of Genomics and Integrative Biology.
‡ DDU Gorakhpur University.

10.1021/jp7102676 CCC: $40.75
Published on Web 05/08/2008

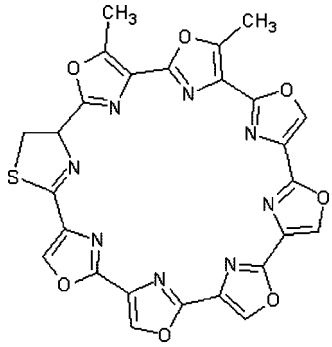

Figure 2. Schematic representation of a telomestatin molecule.

ions.[31] In contrast, Ambrus et al. showed by 1D NMR analysis that, in the presence of K^+ ions, the Tel-22 sequence adopts two conformations, which were found to be the antiparallel and mixed hybrid-type G-quadruplexes according to CD data.[27a] The antiparallel quadruplex can further exist in two forms, namely, the basket-type and the chair-type. Because these two forms give spectrally indistinguishable CD signals,[27a,30] it becomes difficult to comment on the actual conformation existing in the presence of K^+ ions.

Telomestatin (Figure 2) has proven to be a potent nontoxic[32] G-quadruplex stabilizing drug that specifically binds to intramolecular quadruplexes with 70-fold higher selectivity over double-stranded DNA.[33] It is a natural product isolated from *Streptomyces amulatus* 3533-sv4 and has a poly-oxazole unit with consecutive 2,4′-linkages as shown in Figure 2.[34] A number of in vitro and in vivo studies[35–37] have shown the involvement of telomestatin in suppression of the telomere length and apoptosis of tumor cells with an IC_{50} value of ∼5 nM,[24] which is much lower than the values of other quadruplex binding agents. An earlier report showed the telomestatin-mediated stabilization of the antiparallel basket-type G-quadruplex configuration through a 1:2 binding stoichiometry.[24] Yet another report suggested that telomestatin converts preformed mixed-type hybrid or mixture of ht G-quadruplexes $[TTAGGG]_4$ exclusively into the antiparallel basket-type quadruplex−telomestatin complex under K^+ ion conditions.[38] Because an X-ray or NMR structure of the quadruplex−telomestatin complex is not available, it is necessary to undertake a detailed structural study of telomestatin with all possible conformations of 22-mer human Tel-22 G-quadruplexes in order to understand the binding behavior of the telomestatin with human Tel-22 G-quadruplexes.

In the present work, we report modeling and simulation studies performed to investigate the interaction of telomestatin with different structural forms of human Tel-22 $5'AG_3[T_2AG_3]_3$ quadruplexes. Because different reports have suggested variable conformations for the Tel-22 quadruplex in the presence of K^+ ions, we used four native quadruplex conformations, viz., parallel propeller-type, antiparallel basket-type, antiparallel chair-type, and mixed hybrid-type, for simulation studies to understand their relative stabilities and interactions with telomestatin in 1:1 and 1:2 binding stoichiometries. Furthermore, to characterize the energetics of the quadruplex−telomestatin interaction, we estimated the absolute free energy, the binding free energy, the entropy, and the change in solvent-accessible surface area resulting changes in the heat capacity accompanying quadruplex−telomestatin complex formation. A few earlier reports based on docking and MD simulations for human Tel-22 quadruplex−drug interactions focused entirely on a single quadruplex conformation,[24,39,40] so this is the first exhaustive study providing detailed insight into the binding interaction of telomestatin with four possible conformations of the human Tel-22 quadruplex in a K^+ environment.

TABLE 1: Summary of the Model Names, Structures, and Production Times of the Human Tel-22 Quadruplexes

model	structure of G-quadruplex	production time (ns)
MC	antiparallel chair-type (modeled)	3
NM	antiparallel basket-type[25]	3
CR	parallel propeller-type[26]	6
MH	mixed hybrid-type[27b]	4.3

TABLE 2: Summary of the Model Names, Structures, and Production Times of the Human Tel-22 Quadruplex−Telomestatin Complexes

model	structure	production time (ns)
CR1	CR with telomestatin bind at site 1	10
CR2	CR with telomestatin bind at site 2	10
CR12	CR with telomestatin bind at sites 1 and 2	3.6
NM1	NM with telomestatin bind at site 1	3
NM2	NM with telomestatin bind at site 2	3
NM12	NM with telomestatin bind at sites 1 and 2	4.8
MC1	MC with telomestatin bind at site 1	5
MC2	MC with telomestatin bind at site 2	3
MC12	MC with telomestatin bind at sites 1 and 2	6
MH1	MH with telomestatin bind at site 1	6
MH2	MH with telomestatin bind at site 2	5.8
MH12	MH with telomestatin bind at sites 1 and 2	6

Methodology

Model Generation. For the quadruplexes, one modeled and three experimental structures were chosen as starting models. The experimental structures included the antiparallel basket-type NMR structure (PDB 143D),[25] the parallel propeller-type X-ray structure (PDB 1KF1),[26] and a 26-mer mixed hybrid-type NMR structure (PDB 2HY9).[27b] For comparison among various conformations, we removed two adenines from each end of the mixed hybrid-type structure (PDB 2HY9).[27b] Because literature findings suggest that Tel-22 can attain the antiparallel chair-type conformation in K^+ solution,[28,30] we modeled this conformation in the absence of any experimental structure for the nucleotide sequence under investigation. To model the antiparallel chair-type conformation, the coordinates of the G-quartet bases were taken from the NMR structure of the Tel-22 G-quadruplex,[25] and the coordinates for the loop bases and backbone were generated using Insight II software. The ff99[41] force field of Amber 8[42] software was used for optimizations to achieve the final conformation. During the optimization, the coordinates of the quartet bases were kept fixed. The nomenclature assigned to the four native Tel-22 quadruplexes and their respective descriptions are provided in Table 1.

The structure of telomestatin was generated using the Discovery studio package (Accelrys, San Diego, CA). The initial model of telomestatin was optimized with GAMESS (General Atomic and Molecular Electronic Structure System) software, and partial charges (Supporting Information, Figure 1A) were derived using the HF/6–31G* basis set followed by RESP calculation in antechamber module of Amber 8 software.[42] The remaining parameters for telomestatin were taken from the Generalized Amber Forcefield (GAFF).[44]

Docking. The optimized structure of telomestatin was docked against the four quadruplexes. Previous reports have shown that telomestatin stacks externally over the extreme G-quartets.[24,38] Hence, we docked the telomestatin molecule manually over the external G-quartets at site 1 (external quartet extreme to the 5′

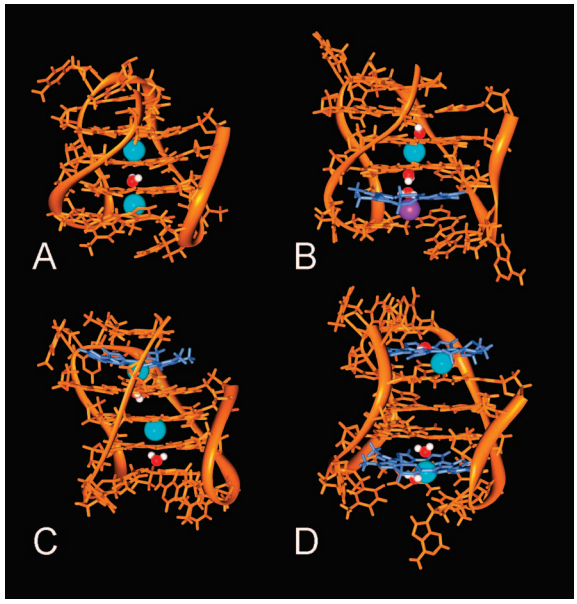

Figure 3. Models of (A) human Tel-22 antiparallel chair-type quadruplex and (B−D) quadruplex−telomestatin complexes shown in orange. Telomestatin (stick model shown in blue) is in complexation with the quadruplex at (B) site 1 and (C) site 2 for a 1:1 stoichiometry and at (D) both sites for a 1:2 stoichiometry. K^+ ions present in the central cavity are shown in cyan. K^+ ions that came from the bulk solution and stabilized near telomestatin during the dynamics runs are shown in purple. Ball-and-stick representations of water molecules are colored by atom type.

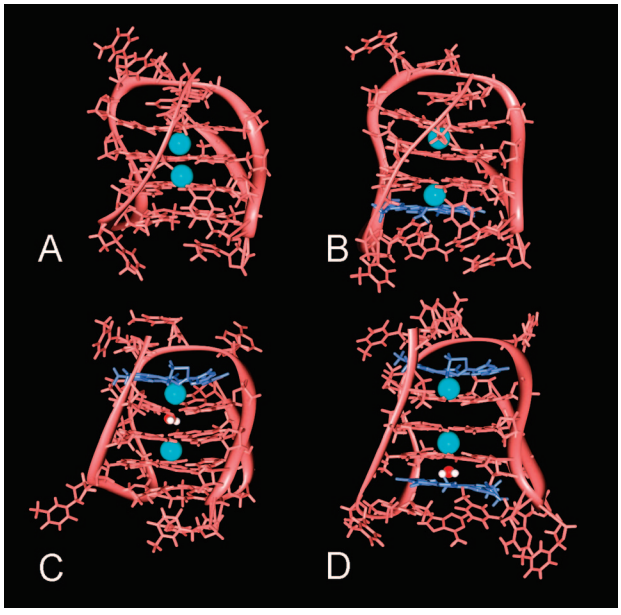

Figure 4. Models of (A) human Tel-22 antiparallel basket-type quadruplex and (B−D) quadruplex−telomestatin complexes shown in pink. Telomestatin (stick model shown in blue) is in complexation with the quadruplex at (B) site 1 and (C) site 2 for a 1:1 stoichiometry and at (D) both sites for a 1:2 stoichiometry. K^+ ions present in the central cavity are shown in cyan. Ball-and-stick representations of water molecules are colored by atom type.

end of oligonucleotide) (Figure 1) and site 2 (external quartet at the 5′ end of oligonucleotide) (Figure 1) individually as well as together at both sites. The orientation and position of telomestatin at the binding site were then refined through a flexible docking approach using the FlexX suite of SYBYL[45] that uses the sybyl scoring function to rank the docked conformations on the basis of energy. Finally, the lowest-energy

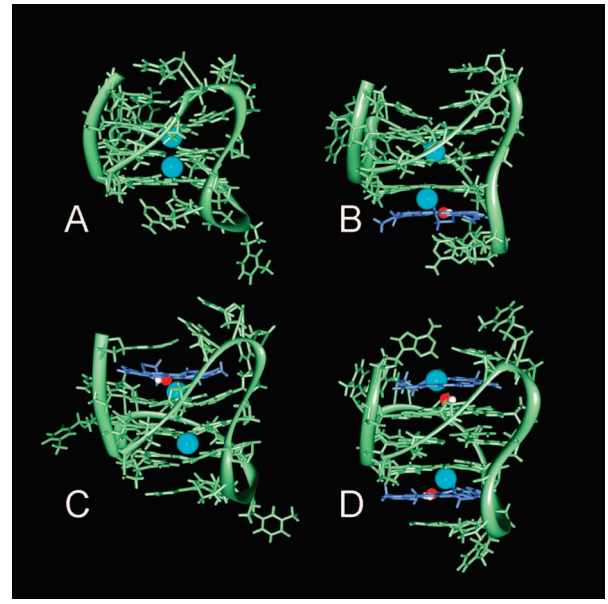

Figure 5. Models of (A) human Tel-22 mixed hybrid-type quadruplex and (B−D) quadruplex−telomestatin complexes shown in light green. Telomestatin (stick model shown in blue) is in complexation with the quadruplex at (B) site 1 and (C) site 2 for a 1:1 stoichiometry and at (D) both sites for a 1:2 stoichiometry. K^+ ions present in the central cavity are shown in cyan. Ball-and-stick representations of water molecules are colored by atom type.

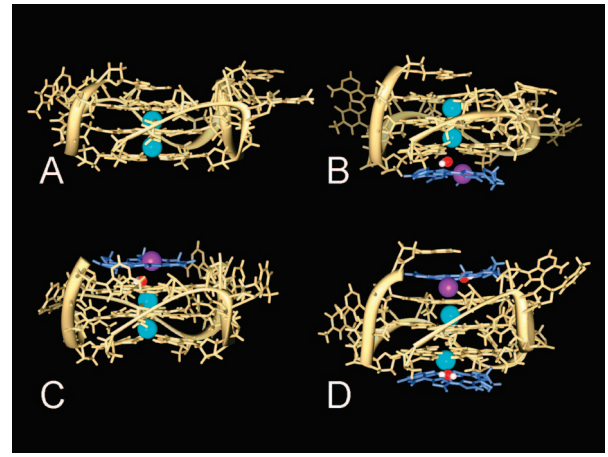

Figure 6. Models of (A) parallel propeller-type quadruplex and (B−D) quadruplex−telomestatin complexes shown in tan. Telomestatin (stick model shown in blue) is in complexation with the quadruplex at (B) site 1 and (C) site 2 for a 1:1 stoichiometry and at (D) both sites for a 1:2 stoichiometry. K^+ ions present in the central cavity are shown in cyan. K^+ ions that came from the bulk solution and stabilized near telomestatin during the dynamics runs are shown in purple. Ball-and-stick representations of water molecules are colored by atom type.

complex conformation was chosen as a starting model. Hence, for each native quadruplex structure, three quadruplex−telomestatin complexes were obtained: one for telomestatin bound at site 1 of the quadruplex, one for telomestatin bound at site 2, and one for telomestatin bound at each site. A total of 12 complex models were generated in this way. Their nomenclature and descriptions are provided in Table 2.

Dynamics. All models including quadruplexes and quadruplex−telomestatin complexes were neutralized with K^+ ions and immersed in a truncated octahedral shell of TIP3P[46] water extending up to 10 Å from the solute. The role of central cations in quadruplex stabilization has been shown by a number of previous studies.[47–49] The X-ray crystal structure of the Tel-22

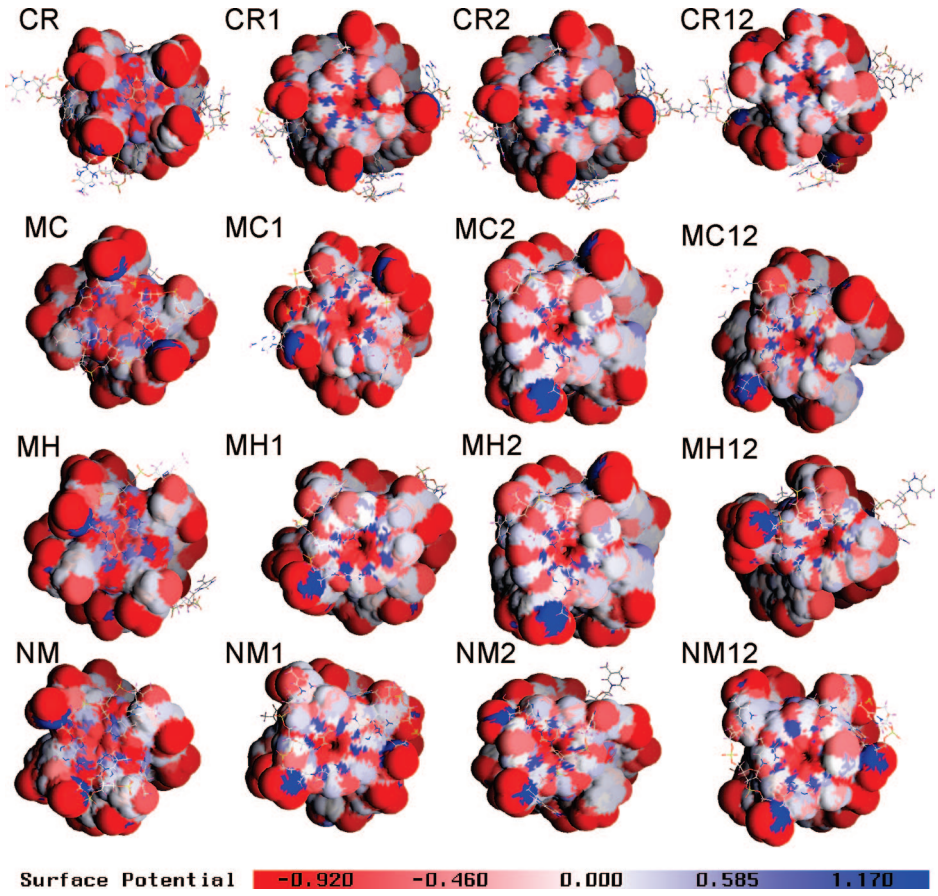

Figure 7. Electrostatic potentials (ESPs) mapped on the solvent-accessible surfaces shown for G-tetrads of the quadruplex and G-tetrads with telomestatin quadruplex−telomestatin complexes. Red represents negative regions, blue represents positive regions, and white represents neutral regions of the molecules. In the central portion of the quadruplex−telomestatin complex, an electronegative pocket (colored red) is formed.

TABLE 3: Average Stacking Distance between Telomestatin and the External G-Quartet for the last 2 ns Trajectory[a]

model	distance (Å)	model	distance (Å)
MH1	3.51	MH12[a]	3.31
MH2	3.40	MC12[a]	3.12
MC1	3.35	NM12[a]	3.43
MC2	3.09	CR12[a]	3.57
NM1	3.21	MH12[b]	3.21
NM2	3.03	MC12[b]	2.80
CR1	3.31	NM12[b]	3.22
CR2	2.85	CR12[b]	2.73

[a] Site 1, external G-quartet extreme to the G-quartet at the 5′ end. [b] Site 2, external G-quartet at the 5′ end.

G-quadruplex[26] contains two K^+ ions in the central cavity. Therefore, we manually placed two K^+ ions in the central channel of all models. All simulations were performed with the Cornell et al. force field[41] ff99 using the sander program of Amber 8. The particle mesh Ewald (PME) method[50] was applied to treat long-range electrostatics using default parameters. A time step of 2 fs and a direct-space nonbonded cutoff of 10 Å were used. The hydrogen bonds were constrained using SHAKE.[51] Temperature regulation was achieved by Langevin coupling[52] with a collision frequency of 1. A constant pressure with isotropic molecule-based scaling with a relaxation time of 1 ps was used.

Equilibration. The solvated structures (both quadruplex and complex) were subjected to multiple initial minimization and dynamics runs to equilibrate the solvent and counter cations. The solute and inner K^+ ions within the quadruplex were initially fixed with force constants of 500 and 50 kcal mol^{-1}, respectively, and were then gradually reduced in subsequent runs. The system was then heated from 0 to 300 K over 25 ps at constant volume and equilibrated for 50 ps at 300 K and a constant pressure of 1 atm that was maintained using Berendsen coupling.[53] A force constant of 50 kcal mol^{-1} was maintained for the solute and inner ions during the heating and equilibration. From this stage, four 50-ps equilibration dynamics runs were performed, and the constraint was slowly reduced by 10 kcal during each run. The final stage of equilibration invoved 1-ns runs using a low 5 kcal mol^{-1} constraint on the solute and inner ions. An unconstrained production phase was then initiated and continued for 3–10 ns (detail are provided in Tables 1 and 2). The structures in the trajectories were collected at 2-ps intervals. All trajectory analysis was done with the Ptraj module in Amber 8.[42] Sybyl7.3[45] and Chimera[54] software were used for molecular visualization. All simulations were performed at the HP Super Computing Facility at the Institute of Genomics and Integrative Biology, New Delhi, India.

Free Energy Calculations. Free energy analysis was performed using the MM_PBSA[55] (Molecular Mechanics, Poisson–Boltzmann, Surface Area) module of Amber 8.[42] Prior to the analysis, all water molecules and potassium ions (except for the two K^+ ions present in the central channel of the G-quadruplex) were stripped from the trajectory. We used a single-trajectory approach to extract 100 snapshots for the quadruplex and quadruplex−telomestatin complexes from the last 2 ns of the trajectory at 20-ps intervals. The Cornell et al. force field[41] was used for gas-phase energies of the solutes with no cutoff. Solvation free energies were computed as sums of polar and nonpolar contributions using a continuum solvent

TABLE 4: Comparison of the Absolute Free Energies[a,b] of the Native Tel-22 G-Quadruplexes

	MC	MH	CR	NM
ΔE_{ELEC}	39.5 (3.52)	−76.89 (3.1)	−80.66 (3.9)	−11.55 (1.97)
ΔE_{VDW}	−228.63 (1.01)	−203.45 (0.95)	−181.2 (1.06)	−234.86 (0.97)
ΔE_{INT}	1064.66 (2.07)	1072.66 (2.19)	1059.18 (2.18)	1060.5 (2.16)
ΔE_{GAS}	875.53 (3.34)	792.33 (3.49)	797.32 (4.11)	814.09 (2.5)
ΔE_{SNP}	19.31 (0.03)	21.05 (0.04)	22.01 (0.03)	19.13 (0.02)
ΔE_{SP}	−5165.5 (4.26)	−5164 (2.79)	−5080.2 (3.41)	−5106.1 (1.64)
ΔE_{SOLV}	−5146.1 (4.26)	−5143 (2.8)	−5058.2 (3.41)	−5087 (1.65)
ΔE_{TOT_ELE}	−5126 (3.39)	−5240.9 (1.15)	−5160.9 (1.41)	−5117.7 (1.19)
$\Delta E_{GAS+SOLV}$	−4270.6 (3.68)	−4350.6 (2.17)	−4260.9 (2.13)	−4272.9 (1.89)
$T\Delta S$	585.7 (0.86)	592.68 (0.7)	602.51 (0.77)	585.13 (0.56)
ΔG_{TOT}	−4862.31	−4943.31	−4863.38	−4858.05

[a] ΔE_{ELEC} = Coulombic energy, ΔE_{VDW} = van der Waals energy, ΔE_{INT} = internal energy, $\Delta E_{GAS} = \Delta E_{ELEC} + \Delta E_{VDW} + \Delta E_{INT}$, ΔE_{SNP} = nonpolar solvation energy, ΔE_{SP} = polar solvation energy, $\Delta E_{SOLV} = \Delta E_{SNP} + \Delta E_{SP}$ = total solvation energy, $\Delta E_{TOT\_ELE} = \Delta E_{ELE} + \Delta E_{SP}$ = total electrostatic energy, $\Delta E_{GAS+SOLV} = \Delta E_{GAS} + \Delta E_{SOLV}$ = enthalpy, $T\Delta S$ = solute entropy, $G_{TOT} = (\Delta E_{GAS+SOLV} - T\Delta S)$ = absolute free energy. [b] All energy values are in kcal mol^{-1}. Standard error of mean (σ_M) given in parentheses.

TABLE 5: Comparison of Free Energies[a,b] of 1:1 Quadruplex−Telomestatin Complexes

	MH1	MH2	CR1	CR2	MC1	MC2	NM1	NM2
ΔE_{ELEC}	−4.89 (0.36)	−51.09 (0.51)	−7.04 (0.42)	−11.63 (0.42)	−92.4 (0.75)	−53.37 (1.08)	−51.49 (0.57)	−63.27 (0.73)
ΔE_{VDW}	−66.68 (0.26)	−66.13 (0.36)	−52.62 (0.14)	−57.63 (0.2)	−84.47 (0.4)	−76.66 (0.37)	−83.66 (0.56)	−73.06 (0.37)
ΔE_{INT}	0 (0)	0 (0)	0 (0)	0 (0)	0 (0)	0 (0)	0 (0)	0 (0)
ΔE_{GAS}	−71.57 (0.39)	−117.22 (0.62)	−59.66 (0.46)	−69.27 (0.45)	−176.87 (0.77)	−130.03 (1.24)	−135.15 (0.83)	−136.33 (0.69)
ΔE_{SNP}	−6.35 (0.02)	−6.51 (0.03)	−4.65 (0.01)	−5.02 (0.02)	−5.7 (0.02)	−7.17 (0.03)	−5.66 (0.03)	−5.12 (0.01)
ΔE_{SP}	40.97 (0.39)	97.82 (0.67)	30.7 (0.43)	37.38 (0.45)	153.34 (0.95)	112.14 (1.75)	109.12 (0.74)	118.24 (0.88)
ΔE_{SOLV}	34.62 (0.38)	91.31 (0.67)	26.05 (0.42)	32.36 (0.44)	147.64 (0.95)	104.97 (1.73)	103.46 (0.73)	113.12 (0.88)
ΔE_{TOT_ELE}	36.08 (0.29)	46.73 (0.38)	23.66 (0.2)	25.74 (0.29)	60.94 (0.65)	58.77 (0.88)	57.63 (0.56)	54.96 (0.42)
$\Delta E_{GAS+SOLV}$	−36.95 (0.27)	−25.91 (0.48)	−33.61 (0.21)	−36.9 (0.28)	−29.23 (0.54)	−25.06 (0.73)	−31.68 (0.55)	−23.21 (0.47)
$T\Delta S$	−22.97 (0.91)	−19.31 (1.2)	−22.18 (1.0)	−20.5 (0.85)	−17.65 (1.38)	−20.67 (1.33)	−19.54 (1.28)	−22.06 (1.09)
ΔG_{TOT}	−13.98	−6.6	−11.43	−16.4	−11.58	−4.39	−12.14	−1.15
$\Delta E_{C\ (GAS+SOLV)}$	−3906 (1.98)	−3910.46 (2.59)	−3916.94 (2.17)	−3914.76 (1.91)	−3882.69 (3.19)	−3899.39 (2.25)	−3906.16 (3.63)	−3905.53 (3.0)
$T\Delta S_{(COM)}$	630.29 (0.66)	642.26 (0.78)	646.83 (0.79)	646.3 (0.69)	636.13 (0.76)	632.58 (0.81)	633.27 (0.9)	632.51 (0.68)
ΔG_{TOT_COM}	−4536.29	−4552.72	−4563.77	−4561.06	−4518.82	−4531.97	−4539.43	−4538.04

[a] ΔE_{ELEC} = Coulombic energy, ΔE_{VDW} = van der Waals energy, ΔE_{INT} = internal energy, $\Delta E_{GAS} = \Delta E_{ELEC} + \Delta E_{VDW} + \Delta E_{INT}$, ΔE_{SNP} = nonpolar solvation energy, ΔE_{SP} = polar solvation energy, $\Delta E_{SOLV} = \Delta E_{SNP} + \Delta E_{SP}$ = total solvation energy, $\Delta E_{TOT\_ELE} = \Delta E_{ELE} + \Delta E_{SP}$ = total electrostatic energy, $\Delta E_{GAS+SOLV} = \Delta E_{GAS} + \Delta E_{SOLV}$ = enthalpy of binding, $T\Delta S$ = solute entropy for binding, $G_{TOT} = (\Delta E_{GAS+SOLV} - T\Delta S)$ = binding free energy, $\Delta E_{C\ (GAS+SOLV)} = \Delta E_{GAS} + \Delta E_{SOLV}$ = enthalpy of complex, $T\Delta S_{(COM)}$ = solute entropy of the complex, $\Delta G_{TOT\_COM} = \Delta E_{C\ (GAS+SOLV)} - T\Delta S_{(COM)}$ = absolute free energy of complex. [b] All energy values are in kcal mol^{-1}. Standard error of mean (σ_M) given in parentheses.

representation. The PBSA program was used to calculate the polar contribution. Values used for the dielectric constant were 1 for the solute and 80 for the surrounding solvent. The Cornell et al. radius set was used to define atom-centered spheres for the solute atoms, and a probe radius of 1.4 Å was used for the solvent to define the dielectric boundary around the molecular surface. The radius for K^+ ions was set at 1.33 Å.[56] A lattice spacing of two grid points per angstrom was used, and 1000 finite-difference iterations were performed. The nonpolar solvent contribution was estimated from a term that depends on the solvent-accessible surface area (SASA), $\Delta G_{snp} = \gamma(\text{SASA}) + \beta$, where γ was set to 0.005 kcal/Å^2 and β to 0. The calculation for the solute entropic contribution was performed with the NMODE module in Amber 8.[42] We used 67 snapshots collected for the last 2 ns of the trajectory at 30-ps intervals. The snapshots were minimized in the gas phase using the conjugate gradient method for 1000 steps, using a distance-dependent dielectric of $4r$ (where r is the interatomic distance) and with a convergence criterion of 0.1 kcal/(mol Å) for the energy gradient. The frequencies of the vibrational modes were computed for these minimized structures at 300 K using the normal-mode analysis methodology.

Solvent-Accessible Surface Area Calculation. The solvent-accessible surface area (SASA) calculations were performed for the lowest-energy structures of each complex using GRASP, version 1.4,[57] with a probe radius of 1.4 Å for the solvent. The surfaces of carbon, carbon-bound hydrogen, and phosphorus was considered to be nonpolar, and the remaining hydrophilic atoms were defined as polar. The calculations were performed with the GRASP radii set using the relation

$$\Delta\text{SASA} = \text{SASA}_{\text{COMPLEX}} - (\text{SASA}_{\text{QUADRUPLEX}} - \text{SASA}_{\text{TELOMESTATIN}}) \quad (1)$$

Results and Discussion

MD simulations of four native quadruplexes and 12 complexes were carried out to explore possible alternative structures of the 22-mer human telomeric quadruplexes and their complexes with telomestatin molecule (Nomenclature is provided in Tables 1 and 2). Tel-22 quadruplexes contain three G-quartet layers stacked over each other with a central channel lined with O6-keto groups. Among the 12 quadruplex−telomestatin complexes, eight have a 1:1 stoichiometry, and four have a 1:2 stoichiometry. There are two 1:1 quadruplex−telomestatin complexes for each of the four native quadruplexes, one with telomestatin bound at site 1 and another with telomestatin bound at site 2, whereas the 1:2 quadruplex−telomestatin complexes had one telomestatin bound at each of the sites.

MD Simulation of Antiparallel Chair-Type Quadruplex and Its Complexes with Telomestatin. The antiparallel chair-type quadruplex and its complexes with telomestatin bound at site 1 (MC1), at site 2 (MC2), and at both sites (MC12) are shown in Figure 3A−D, respectively. The root mean square

TABLE 6: Comparison of Free Energies[a,b] of the 1:2 Quadruplex−Telomestatin Complexes

	MH12	CR12	MC12	NM12
ΔE_{ELEC}	−45.69 (1.23)	−41.71 (0.80)	−146.25 (0.9)	−68.38 (0.93)
ΔE_{VDW}	−133.61 (0.47)	−106.65 (0.56)	−152.58 (0.49)	−140.06 (0.44)
ΔE_{INT}	0 (0)	0 (0)	0 (0)	0 (0)
ΔE_{GAS}	−179.3 (1.25)	−148.36 (1.11)	−298.83 (0.82)	−208.44 (0.87)
ΔE_{SNP}	−12.47 (0.04)	−9.63 (0.06)	−14.59 (0.02)	−9.71 (0.02)
ΔE_{SP}	132.31 (1.67)	104.45 (0.87)	271.33 (1.03)	167.58 (0.93)
ΔE_{SOLV}	119.84 (1.67)	94.82 (0.84)	256.74 (1.04)	157.88 (0.93)
ΔE_{TOT_ELE}	86.62 (0.72)	62.75 (0.47)	125.08 (0.7)	99.2 (0.79)
$\Delta E_{GAS+SOLV}$	−59.46 (0.79)	−53.53 (0.63)	−42.09 (0.67)	−50.56 (0.67)
$T\Delta S$	−35.63 (1.65)	−30.17 (1.40)	−32.44 (1.70)	−31.91 (1.70)
ΔG_{TOT}	−23.83	−23.36	−9.65	−18.65
$\Delta E_{C\,(GAS+SOLV)}$	−3547.98 (2.63)	−3562.21 (2.65)	−3528.71 (5.85)	−3559.68 (4.40)
$T\Delta S_{(COM)}$	680.85 (0.89)	691 (0.92)	681.82 (1.01)	685.7 (0.93)
ΔG_{TOT_COM}	−4228.83	−4253.21	−4210.53	−4245.38

[a] ΔE_{ELEC} = Coulombic energy, ΔE_{VDW} = van der Waals energy, ΔE_{INT} = internal energy, $\Delta E_{GAS} = \Delta E_{ELEC} + \Delta E_{VDW} + \Delta E_{INT}$, ΔE_{SNP} = nonpolar solvation energy, ΔE_{SP} = polar solvation energy, $\Delta E_{SOLV} = \Delta E_{SNP} + \Delta E_{SP}$ = total solvation energy, $\Delta E_{TOT\_ELE} = \Delta E_{ELE} + \Delta E_{SP}$ = total electrostatic energy, $\Delta E_{GAS+SOLV} = \Delta E_{GAS} + \Delta E_{SOLV}$ = enthalpy of binding, $T\Delta S$ = solute entropy for binding, $\Delta G_{TOT} = \Delta E_{GAS+SOLV} - T\Delta S$ = binding free energy, $\Delta E_{C\,(GAS+SOLV)} = \Delta E_{GAS} + \Delta E_{SOLV}$ = enthalpy of the complex, $T\Delta S_{(COM)}$ = solute entropy of the complex, $\Delta G_{TOT\_COM} = \Delta E_{C\,(GAS+SOLV)} - T\Delta S_{(COM)}$ = absolute free energy of the complex. [b] All energy values are in kcal mol^{-1}. Standard error of mean (σ_M) given in parentheses.

TABLE 7: Calculations of Change in Solvent-Accessible Surface Area[a] Due to Quadruplex−Telomestatin Complex Formation

	$SASA_{COMPLEX}$			$SASA_{QUADRUPLEX}$			$SASA_{TELOMESTATIN}$					
	A_P	A_{NP}	A_{TOT}	A_P	A_{NP}	A_{TOT}	A_P	A_{NP}	A_{TOT}	ΔA_P[a]	ΔA_{NP}[b]	ΔA_{TOT}[c]
MC12	2888	1793	4681	3262	1927	5189	643	898	1541	−1017	−1032	−2049
NM12	3650	1146	4797	4011	1241	5252	647	885	1532	−1008	−979	−1987
MH12	3111	1719	4830	3383	1754	5136	645	899	1545	−917	−934	−1851
CR12	3098	1794	4892	3153	1624	4777	647	901	1548	−702	−731	−1432
NM1	2617	1496	4113	2840	1652	4492	321	444	765	−544	−600	−1144
MC2	2901	1646	4547	3129	1766	4894	322	448	770	−549	−568	−1117
NM2	2804	1607	4411	3024	1682	4706	325	454	779	−546	−528	−1074
MC1	2680	1542	4222	2862	1587	4449	321	444	765	−503	−489	−992
MH1	2891	1457	4348	3037	1460	4497	322	450	772	−468	−453	−921
MH2	2922	1534	4456	3030	1576	4606	316	449	765	−423	−491	−914
CR2	2928	1596	4524	2941	1492	4434	325	442	767	−338	−339	−677
CR1	3103	1693	4797	3065	1588	4653	325	441	766	−287	−336	−623

[a] A_P = polar area, A_{NP} = non-polar area, A_{TOT} = total area. [b] Change in polar area (ΔA_P) = $A_{P(COMPLEX)} - A_{P(QUADRUPLEX)} - A_{P(TELOMESTATIN)}$. [c] Change in nonpolar area (ΔA_{NP}) = $A_{NP(COMPLEX)} - A_{NP(QUADRUPLEX)} - A_{NP(TELOMESTATIN)}$. [d] Change in total area (ΔA_{TOT}) = $A_{TOT(COMPLEX)} - A_{TOT(QUADRUPLEX)} - A_{TOT(TELOMESTATIN)}$.

TABLE 8: Calculation of the Change in Heat Capacity (ΔC_p) Due to the Change in the Solvent-Accessible Surface Area

model	ΔC_p[63]
MC12	−271 ± 51
NM12	−252 ± 52
MH12	−246 ± 46
CR12	−194 ± 35
NM1	−164 ± 26
MC2	−150 ± 28
MH2	−136 ± 26
NM2	−136 ± 20
MC1	−126 ± 28
MH1	−117 ± 26
CR1	−94 ± 24
CR2	−89 ± 13

deviation (rmsd) values were found to be <1.7 Å for the heavy atoms of the guanine quartets, <3.5 Å for all atoms of the quadruplex, and ~0.6 Å for all atoms of telomestatin (Supporting Information, Figure SII1A−D). Investigation of the MC model trajectory showed that one central K^+ ion was exchanged with a water molecule and stabilized between thymine bases of two lateral loops and external quartet. Both the shifted ion and the water molecule remained at their occupied positions for the rest of the production dynamics run. In complex MC1, one K^+ ion was derived from the bulk solution near the bound telomestatin, and a central K^+ ion moved into the bulk solution from site 2. One central K^+ ion in complex MC2 and both central K^+ ions in complex MC12 were shifted and stabilized in the space between telomestatin and the subsequent quartet.

MD Simulation of Antiparallel Basket-Type Quadruplex and Its Complexes with Telomestatin. The native antiparallel basket-type quadruplex (NM) and its complexes with telomestatin bound at site 1 (NM1), site 2 (NM2), and both sites 1 and 2 (NM12) (Figure 4A−D, respectively) exhibited rmsd values of <1.5 Å for the heavy atoms of the guanine quartets, <4.0 Å for all atoms of the quadruplex, and 0.5 Å for all atoms of telomestatin (Supporting Information, Figure SII2A−D). The central K^+ ions remained at their respective positions in the NM quadruplex, whereas in complexes NM1 and NM2, one central K^+ ion shifted to the space between bound telomestatin and the subsequent quartet. Complex NM12 (1:2 stoichiometry) exhibited a shift of only a single K^+ ion from the central cavity of the quadruplex, whereas the other ion remained between the consecutive quartets. This might be due to the lack of a passage for central K^+ ion movement owing to steric hindrance presented by the external quartet, which might be enhanced as a result of the compaction produced by the stretching of the diagonal loop due to the binding of telomestatin.

MD Simulation of Mixed Hybrid-Type Quadruplex and Its Complexes with Telomestatin. The mixed hybrid-type quadruplex (MH) and its complexes with telomestatin bound at site 1 (MH1), site 2 (MH2), and both sites 1 and 2 (MH12) (Figure 5A−D, respectively) exhibited rmsd values of <1.0 Å for the heavy atoms of the guanine quartets, <4.0 Å for all atoms of the quadruplex, and 0.5 Å for all atoms of telomestatin (Supporting Information, Figure SII3A−D). No ion shifting was observed for the MH model, whereas all of the three complexes showed the shifting of one or both central K^+ ions to the space between the external quartet and the bound telomestatin.

MD Simulation of Parallel Propeller-Type Quadruplex and Its Complexes with Telomestatin. We also investigated the parallel propeller-type quadruplex (CR) and its three complexes with telomestatin bound at site 1 (CR1), site 2 (CR2), and both sites 1 and 2 (CR12) (Figure 6A−D, respectively). All of the models were stable during the dynamics runs and exhibited rmsd values of ∼0.5 Å for the heavy atoms of the G-quartets, < 4.5 Å for all atoms of the quadruplex, and ∼0.5 Å for all atoms of telomestatin in the parallel propeller-type quadruplex−telomestatin complexes (Supporting Information, Figure SII4A−D). In models CR1 and CR2, one K^+ ion from the bulk solution was observed to stabilize near telomestatin. In model CR12, one of the central K^+ ions shifted to site 1, whereas the other remained at the native position. An additional K^+ ion from the bulk solution was found to stabilize near the telomestatin bound at site 2 of model CR12 (Figure 6D).

Overall, the analysis indicated that, during the dynamics runs, the K^+ ion residing between telomestatin and the quartet either shifted from the central cavity of the quadruplex or was derived from the surrounding solution. The stabilization of one K^+ ion between telomestatin and the external quartet might be due to the formation of an electronegative pocket created by the presence of the eight nitrogen atoms of telomestatin and the four O6 atoms of the guanine bases of the subsequent quartet. To further confirm this hypothesis, we mapped the electrostatic potentials (ESPs) on the solvent-accessible surfaces of the G-quartets for all quadruplexes and quadruplex−telomestatin complexes using GRASP[57] software as shown in Figure 7. The charges used for mapping the electrostatic potentials were the same as those used for the simulations. In the central portion of the quadruplex−telomestatin complex, an electronegative pocket (negatively charged surface, red colored) can be seen in Figure 7, which seems to be the most probable reason for K^+ ion stabilization.

The stable trajectories of all of the models shown through rmsd plots (Supporting Information, Figure 2) indicated that the MD simulations converged. The potential, kinetic, and total energies were stable throughout the production dynamics runs (Supporting Information, Figure 3), which supports the stability of production-phase dynamics. Further, to check quadruplex−telomestatin stacking interactions, we calculated the average distance between telomestatin and the subsequent quartet for the last 2 ns of the trajectory at 100-ps intervals. The average distances between telomestatin and the subsequent quartet of both the 1:1 and 1:2 complexes ranged between 2.80 to 3.57 Å (Table 3). The average distance between telomestatin and the subsequent quartet was comparable to the 3.4 Å[58] average distance between consecutive quartets of the quadruplex. These distances suggest strong van der Waals interactions between the large surfaces of telomestatin and the G-quartet.

Energetics of Quadruplex Stabilization. The absolute free energy components for the quadruplex models of Tel-22 are summarized in Table 4. The total energy of the solute (ΔE_{GAS}) includes the electrostatic energy, the van der Waals energy derived from a Lennard-Jones potential, and the internal energy. The nonpolar contribution of the solvation energy was calculated from the solvent-accessible surface area of the molecule. Finite-difference Poisson–Boltzmann equations were used to calculate the electrostatic potential field. Stelf et al.[59] demonstrated previously that free energy calculations can provide meaningful results only with explicit inclusion of the central bound ions. A few other studies have also emphasized the importance of ion inclusion for MM_PBSA calculations.[60–62] Hence, we carried out energy calculations with the two K^+ ions present in the central channel of the G-quadruplex. The absolute free energy calculations for the quadruplex suggested a favorable contribution from solute electrostatics (ΔE_{ELEC}) for all native quadruplex models except MC. In addition, a favorable contribution was also found for the van der Waals energy ($\Delta E_{VDW.}$). The solute entropy cost for the native quadruplex models ($T\Delta S$) ranged from 585.13 to 602.51 kcal mol^{-1} and therefore contributed favorably to the absolute free energy. The absolute free energy (ΔG_{TOT}) of the native quadruplex models ranged between −4858.05 and −4943.31 kcal mol^{-1}. These absolute free energy values show that the mixed hybrid-type conformation is more stable than the other native G-quadruplex models because it has the lowest absolute free energy (−4943.31 kcal mol^{-1}).

Energetics of Quadruplex−Telomestatin Interactions. The free energy components for the telomestatin interaction with all four quadruplex structures in both the 1:1 and 1:2 ratios are summarized in Tables 5 and 6. For both the 1:1 and 1:2 quadruplex−telomestatin complexes, the electrostatic energy (ΔE_{ELEC}) and the van der Waals energy (ΔE_{VDW}) provide favorable contributions. In addition, the nonpolar solvation energy (ΔE_{SNP}) also contributes favorably to the total binding free energy. This implies that electrostatic energy, van der Waals energy, and nonpolar solvation energy are important contributors to quadruplex−telomestatin binding. The solvent electrostatic energy (ΔE_{SP}) makes an unfavorable contribution. Moreover, we observed unfavorable entropic contributions ($T\Delta S$) for all telomestatin-quadruplex binding models.

The energy calculations show negative binding free energies for the 1:1 binding stoichiometry, ranging from −1.15 to −16.4 kcal mol^{-1} (Table 5). The binding free energies for the 1:1 complexes suggest that telomestatin can bind to all of the quadruplex conformations. However, the lowest binding free energy for the CR2 model suggests that telomestatin binds most efficiently at site 2 of the parallel propeller-type G-quadruplex. The solute entropy for complexes $(T\Delta S)_{COM}$ show favorable contributions. The absolute free energy of the 1:1 quadruplex−telomestatin complexes range from −4518.82 to −4563.77 kcal mol^{-1}. The absolute free energies suggest that models CR1 and CR2 exhibit better stability than the other 1:1 quadruplex−telomestatin complex models.

The binding free energies (ΔG_{TOT}) for the 1:2 quadruplex−telomestatin binding stoichiometry range from –9.65 to –23.83 kcal mol^{-1}. Models MH12 and CR12 exhibited similar binding free energies of –23.83 and –23.36 kcal mol^{-1}, respectively. These binding free energies for models MH12 and CR12 suggest that telomestatin binds with almost the same strength to both conformations. The absolute free energies for the 1:2 quadruplex−telomestatin complex models range from −4210.53 to −4253.21 kcal mol^{-1}. These calculations suggest a greater stability for model CR12 because it has the lowest absolute free energy (−4253.21 kcal mol^{-1}) among the 1:2 quadruplex−telomestatin complex models. The overall analysis shows that models with a 1:2 binding stoichiometry have lower binding free energies

than those with a 1:1 binding stoichiometry, which suggests that 1:2 quadruplex−telomestatin complexation is preferred over 1:1 quadruplex−telomestatin complexation.

A macromolecular system exhibits numerous microstates. Therefore, for free energy calculations of a macromolecular system, the only practical approach is to consider a limited numbers of snapshots. For the present energy calculations, increasing the number of snapshots from 67 (at 30-ps intervals for the last 2 ns of the trajectory; data not provided) to 100 (at 20-ps intervals for the last 2 ns of the trajectory) caused the free energies to vary only slightly and remained within the range of standard error. Therefore, we did not increase the number of snapshots further for the calculations. The low values of the standard error of the mean for both the free energy and entropy calculations suggest that the energy calculations were numerically stable.

Analysis of Solvent-Accessible Surface Area and Heat Capacity Change. Binding of telomestatin to the external G-quartets of the Tel-22 quadruplex reduces the total solvent-accessible surface area (SASA) of the complex. The last column of Table 7 shows reductions in solvent-accessible surface area (ΔSASA) ranging from −623 to −1144 Å^2 upon 1:1 quadruplex−telomestatin complex formation and from −1432 to −2049 Å^2 upon 1:2 quadruplex−telomestatin complex formation (Table 7). The reductions in polar (ΔA_P) and nonpolar (ΔA_{NP}) surface areas did not vary significantly. This can be attributed to the large surface area of telomestatin, containing ∼42% polar and ∼58% nonpolar surfaces, whereby both types contribute equally in the total reduction of the solvent-accessible surface area. Chaires' group proposed an empirical relation (eq 2)[63] to calculate the change in heat capacity from the changes in polar (ΔA_P) and nonpolar (ΔA_{NP}) surface areas of nucleotides due to ligand binding

$$\Delta C_p = (0.982 \pm 0.026)\Delta A_{NP} - (0.121 \pm 0.077)\Delta A_P \quad (2)$$

The change in heat capacity (ΔC_p) is a measure of hydration changes during a reaction and is directly correlated with solvent exchange. ΔC_p can be used to estimate the extent of dissolution or exposure of polar and nonpolar groups during complex formation. A negative value of ΔC_p implies dissolution of the nonpolar surface area upon quadruplex−telomestatin complex formation, whereas a positive value of ΔC_p implies dissolution of polar surface area. All of the ΔC_p values were found to be negative and to lie between -89 ± 13 and -271 ± 51 cal mol^{-1} K^{-1} (Table 8). The negative ΔC_p values for quadruplex−telomestatin complex formation imply that the positive contribution due to polar surface burial is compensated by corresponding burial of nonpolar surface area. Experimental determinations of ΔC_p for duplex−ligand interactions are well-documented in the literature, but such data on quadruplex−ligand interactions are sparse. For both intercalative and minor-groove binding ligands, it was shown that ΔC_p values vary from –100 to –400 cal mol^{-1} K^{-1}.[63,64] The only reported ΔC_p value for the quadruplex−ligand interaction is available for porphyrin (TMPyP4) binding to c-MYC quadruplex.[65] The ΔC_p values obtained for binding of TMPyP4 at two sites of c-MYC 27-mer quadruplex are 31 and 58 cal mol^{-1} K^{-1}, respectively.[65] Recently, we also determined the ΔC_p value for berberine binding to Tel-22 quadruplex by means of isothermal calorimetry (ITC). Enthalpy changes (ΔH_b) for the binding of berberine to Tel-22 quadruplex as a function of temperature were measured, and the slope of a plot of ΔH_b vs temperature yielded a ΔC_p value of -94 ± 5 cal mol^{-1} K^{-1} for the binding of berberine to quadruplex (unpublished work). These studies show that the ΔC_p values for quadruplex−ligand interactions are less negative than the ΔC_p values for known duplex−ligand interactions. This might be a thermodynamic signature for quadruplex−ligand interaction. Experimental determinations of changes in heat capacity associated with ligand−macromolecule binding can help to explain the driving forces for the binding reactions of drug–DNA complexes. As telomestatin is hydrophobic in nature and has a poor solubility in water, it is quite difficult to experimentally assess the thermodynamic parameters governing its interaction with the quadruplex. On the other hand, telomestatin is one of the most exciting natural ligand that binds to the quadruplex with high affinity and great selectivity. Thus, the thermodynamic parameters obtained from this study certainly have merit in explaining the selectivity of telomestatin for the quadruplex and have crucial role to play in the field of quadruplex−ligand interactions.

Conclusion

This study explains the relative stability of Tel-22 G-quadruplex configurations and adds to the understanding of quadruplex−telomestatin interactions. MD simulations were performed for four native quadruplex configurations and 12 quadruplex−telomestatin complexes with both 1:1 and 1:2 binding stoichiometries. The energy calculations suggested that the mixed hybrid-type conformation is the most stable among native quadruplexes. The quadruplex−telomestatin complexes seem to be stable in the parallel propeller-type conformation in both 1:1 and 1:2 binding stoichiometries. The binding free energies suggest better binding for the 1:2 binding stoichiometry than for the 1:1 binding stoichiometry for quadruplex−telomestatin complexes. Overall, our data indicated that K^+ ion stabilization near telomestatin adds uniqueness to the quadruplex−telomestatin interactions with Tel-22 G-quadruplex and calls for further study on the effects of ions on binding. The increased tendency of human Tel-22 G-quadruplex to adopt multiple conformations under varying environmental conditions poses a significant challenge in the appropriate design of conformation-specific drugs that could efficiently bind and stabilize the structure. A study such as ours provides in-depth insight into the conformational aspects of the quadruplex and further evaluates its respective interactions with drugs.

Acknowledgment. S.A. acknowledges a CSIR Diamond Jubilee Research Intern Award Fellowship from CSIR. The authors acknowledge CSIR for funding (CMM0017) this research. The authors also thank Professor David A. Case, The Scripps Research Institute, La Jolla, CA, for providing a complementary copy of Amber 8.

Supporting Information Available: Plots of rmsd vs time; plots of kinetic energy, potential energy, and total energy vs time; a telomestatin figure with a table showing partial charges. This material is available free of charge via the Internet at http://pubs.acs.org.

References and Notes

(1) Wright, W. E.; Tesmer, V. M.; Huffman, K. E.; Levene, S. D.; Shay, J. W. *Genes Dev.* **1997**, *11*, 2801–2809.
(2) Makarov, V. L.; Hirose, Y.; Langmore, J. P. *Cell* **1997**, *88*, 657–666.
(3) McElligott, R.; Wellinger, R. J. *EMBO J.* **1997**, *16*, 3705–3714.
(4) Smogorzewska, A.; de Lange, T. *Annu. Rev. Biochem.* **2004**, *73*, 177–208.
(5) Harley, C. B.; Futcher, A. B.; Greider, C. W. *Nature* **1990**, *345*, 458–460.
(6) Bodnar, A. G.; Ouellette, M.; Frolkis, M.; Holt, S. E.; Chiu, C. P.; Morin, G. B.; Harley, C. B.; Shay, J. W.; Lichtsteiner, S.; Wright, W. E. *Science* **1998**, *279*, 349–352.

(7) Neidle, S.; Read, M. A. *Biopolymers* **2001**, *56*, 195–208.
(8) Blackburn, E. H. *Cell* **1994**, *77*, 621–723.
(9) Sun, D.; Thompson, B.; Cathers, B. E.; Salazar, M.; Kerwin, S. M.; Trent, J. O.; Jenkins, T. C.; Neidle, S. *J. Med. Chem.* **1997**, *40*, 2113–2116.
(10) White, L. K.; Wright, W. E.; Shay, J. W. *Biotechnology* **2001**, *19*, 114–120.
(11) Mergny, J.-L.; Riou, J.-F.; Maillet, P.; Teulade-Fichou, M.-P.; Gilson, E. *Nucleic Acids Res.* **2002**, *30*, 839–865.
(12) Neidle, S.; Parkinson, G. N. *Nat. Rev. Drug Discovery* **2002**, *1*, 383–393.
(13) Perry, P. J.; Read, M. A.; Davies, R. T.; Gowan, S. M.; Reszka, A. P.; Wood, A. A.; Kelland, L. R.; Neidle, S. *J. Med. Chem.* **1999**, *42*, 2679–2684.
(14) Read, M. A.; Wood, A. A.; Harrison, R. J.; Gowan, S. M.; Kelland, L. R.; Dosanjh, H. S.; Neidle, S. *J. Med. Chem.* **1999**, *42*, 4538–4546.
(15) Read, M.; Harrison, R. J.; Romagnoli, B.; Tanious, F. A.; Gowan, S. H.; Reszka, A. P.; Wilson, W. D.; Kelland, L. R.; Neidle, S. *Proc. Natl. Acad. Sci. U.S.A.* **2001**, *98*, 4844–4849.
(16) Han, H.; Cliff, C. L.; Hurley, L. H. *Biochemistry* **1999**, *38*, 6981–6986.
(17) Fedoroff, O. Y.; Salazar, M.; Han, H.; Chemeris, V. V.; Kerwin, S. M.; Hurley, L. H. *Biochemistry* **1998**, *37*, 12367–12374.
(18) Rangan, A.; Fedoroff, O. Y.; Hurley, L. H. *J. Biol. Chem.* **2001**, *276*, 4640–4646.
(19) Harrison, R. J.; Gowan, S. M.; Kelland, L. R.; Neidle, S. *Bioorg. Med. Chem. Lett.* **1999**, *9*, 2463–2468.
(20) Wheelhouse, R. T.; Sun, D.; Han, H.; Han, F. X.; Hurley, L. H. *J. Am. Chem. Soc.* **1998**, *120*, 3261–3262.
(21) Han, F. X.; Wheelhouse, R. T.; Hurley, L. H. *J. Am. Chem. Soc.* **1999**, *121*, 3561–3570.
(22) Han, H.; Rangan, A.; Langley, D. R.; Hurley, L. H. *J. Am. Chem. Soc.* **2001**, *123*, 8902–8913.
(23) Shi, D.-F.; Wheelhouse, R. T.; Sun, D.; Hurley, L. H. *J. Med. Chem.* **2001**, *44*, 4509–4523.
(24) Kim, M.-Y.; Vankayalapati, H.; Shin-Ya, K.; Wierzba, K.; Hurley, L. H. *J. Am. Chem. Soc.* **2002**, *124*, 2098–2099.
(25) Wang, Y.; Patel, D. J. *Structure* **1993**, *1*, 263–282.
(26) Parkinson, G. N.; Lee, M. P.; Neidle, S. *Nature* **2002**, *417*, 876–880.
(27) (a) Ambrus, A.; Chen, D.; Dai, J.; Bialis, T.; Jones, R. A.; Yang, D. *Nucleic Acids Res.* **2006**, *34*, 2723–2735. (b) Dai, J.; Punchihewa, C.; Ambrus, A.; Chen, D.; Jones, R. A.; Yang, D. *Nucleic Acids Res.* **2007**, *35*, 2440–2450.
(28) He, Y.; Neumann, R. D.; Panyutin, I. G. *Nucleic Acids Res.* **2004**, *32*, 5359–5367.
(29) Redon, S.; Bombard, S.; Elizondo-Riojas, M. A.; Chottard, J. C. *Nucleic Acids Res.* **2003**, *31*, 1605–1613.
(30) Qi, J.; Shafer, R. H. *Nucleic Acids Res.* **2005**, *33*, 3185–3192.
(31) Li, J.; Correia, J. J.; Wang, L.; Trent, J. O.; Chaires, J. B. *Nucleic Acids Res.* **2005**, *33*, 4649–4659.
(32) Tauchi, T.; Shin-Ya, K.; Sashida, G.; Sumi, M.; Okabe, S.; Ohyashiki, J. H.; Ohyashiki, K. *Oncogene* **2006**, *25*, 5719–5725.
(33) Kim, M.-Y.; Gleason-Guzman, M.; Izbicka, E.; Nishioka, D.; Hurley, L. H. *Cancer Res.* **2003**, *63*, 3247–3256.
(34) Shin-Ya, K.; Wierzba, K.; Matsuo, K. L.; Ohtani, T.; Yamada, Y.; Furihata, K.; Hayakawa, Y.; Seto, H. *J. Am. Chem. Soc.* **2001**, *123*, 1262–1263.
(35) Long, S.; Argyle, D. J.; Gault, E. A.; Nasir, L. *Vet. Comp. Oncol.* **2007**, *5*, 99–107.
(36) (a) Gomez, D.; Wenner, T.; Brassart, B.; Douarre, C.; O'Donohue, M. F.; El Khoury, V.; Shin-Ya, K.; Morjani, H.; Trentesaux, C.; Riou, J. F. *J. Biol. Chem.* **2006**, *281*, 38721–38729. (b) Gomez, D.; O'Donohue, M. F.; Wenner, T.; Douarre, C.; Macadre, J.; Koebel, P.; Giraud-Panis, M. J.; Kaplan, H.; Kolkes, A.; Shin-Ya, K.; Riou, J. F. *Cancer Res.* **2006**, *66*, 6908–6912.
(37) Binz, N.; Shalaby, T.; Rivera, P.; Shin-Ya, K.; Grotzer, M. A. *Eur. J. Cancer.* **2005**, *41*, 2873–2881.
(38) Rezler, E. M.; Seenisamy, J.; Bashyam, S.; Kim, M. Y.; White, E.; Wilson, W. D.; Hurley, L. H. *J. Am. Chem. Soc.* **2005**, *127*, 9439–9447.
(39) Ishikawa, Y.; Tomisugi, Y.; Uno, T. *Nucleic Acids Symp. Ser. (Oxford)* **2006**, *50*, 331–332.
(40) Yang, D.-Y.; Chang, T.-C.; Sheu, S.-Y. *J. Phys. Chem. A.* **2007**, *111*, 9224–9232.
(41) Cornell, W. D.; Cieplak, P.; Bayly, C. I.; Gould, I. R., Jr.; Ferguson, D. M.; Spellmeyer, D. C.; Fox, T.; Caldwell, J. W.; Kollman, P. A. *J. Am. Chem. Soc.* **1995**, *117*, 5179–5197.
(42) Case, D. A.; Darden, T. A.; Cheatham, T. E., III; Simmerling, C. L.; Wang, J.; Duke, R. E.; Luo, R.; Merz, K. M.; Wang, B.; Pearlman, D. A.; Crowley, M.; Brozell, S.; Tsui, V.; Gohlke, H.; Mongan, J.; Hornak, V.; Cui, G.; Beroza, P.; Schafmeister, C.; Caldwell, J. W.; Ross, W. S.; Kollman, P. A. *Amber 8*; University of California: San Francisco, CA, 2004.
(43) Schmidt, M. W.; Baldridge, K. K.; Boatz, J. A.; Elbert, S. T.; Gordon, M. S.; Jensen, J. H.; Koseki, S.; Matsunaga, N.; Nguyen, K. A.; Su, S.; Windus, T. L.; Dupuis, M.; Montgomery, J. A. *J. Comput. Chem.* **1993**, *14*, 1347–1363.
(44) Wang, J.; Wolf, R. M.; Caldwell, J. W.; Kollman, P. A.; Case, D. A. *J. Comput. Chem.* **2004**, *25*, 1157–1174.
(45) *SYBYL 7.3*; Tripos International: St. Louis, MO, 2006.
(46) Jorgensen, W. L.; Chandrasekhar, J.; Madura, J. D.; Impey, R. W.; Klein, M. L. *J. Chem. Phys.* **1983**, *79*, 926–935.
(47) Pinnavaia, T. J.; Marshall, C. L.; Mettler, C. M.; Fisk, C. L.; Miles, H. T.; Becker, E. D. *J. Am. Chem. Soc.* **1978**, *100*, 3625–3627.
(48) Howard, F. B.; Miles, H. T. *Biochemistry* **1982**, *21*, 6736–6745.
(49) Strahan, G. D.; Keniry, M. A.; Shafer, R. H. *Biophys. J.* **1998**, *75*, 968–981.
(50) Darden, T.; York, D.; Pedersen, L. *J. Chem. Phys.* **1993**, *98*, 10089–10092.
(51) Ryckaert, J. P.; Ciccotti, G.; Berendsen, H. J. C. *J. Comput. Phys.* **1977**, *23*, 327–341.
(52) Izaguirre, J. A.; Catarello, D. P.; Wozniak, J. M.; Skeel, R. D. *J. Chem. Phys.* **2001**, *114*, 2090–2098.
(53) Berendsen, H. J. C.; Postma, J. P. M.; van Gunsteren, W. F.; DiNola, A.; Haak, J. R. *J. Chem. Phys.* **1984**, *81*, 3684–3690.
(54) Pettersen, E. F.; Goddard, T. D.; Huang, C. C.; Couch, G. S.; Greenblatt, D. M.; Meng, E. C.; Ferrin, T. E. *J. Comput. Chem.* **2004**, *25*, 1605–1612.
(55) Gohlke, H.; Case, D. A. *J. Comput. Chem.* **2003**, *25*, 238–250.
(56) Pauling, L. *Ions Ionic Cryst.* **1927**, *49*, 765–790.
(57) Nicholls, A.; Sharp, K. A.; Honig, B. *Proteins: Struct. Funct. Genet.* **1991**, *11*, 281–296.
(58) Gellert, M.; Lipsett, M. N.; Davies, D. R. *Proc. Natl. Acad. Sci. U.S.A.* **1962**, *48*, 2013–2018.
(59) Stefl, R.; Cheatham, T. E., III; Spackova, N.; Fadrna, E.; Berger, I.; Koca, J.; Jir1, S. *Biophys. J.* **2003**, *85*, 1787–1804.
(60) Jayaram, B.; Sprous, D.; Young, M. A.; Beveridge, D. L. *J. Am. Chem. Soc.* **1998**, *120*, 10629–10633.
(61) Sprous, D.; Young, M. A.; Beveridge, D. L. *J. Phys. Chem. B.* **1998**, *102*, 4658–4667.
(62) Tsui, V.; Case, D. A. *J. Phys. Chem. B.* **2001**, *105*, 11314–11325.
(63) Ren, J.; Jenkins, T. C.; Chaires, J. B. *Biochemistry* **2000**, *39*, 8439–8447.
(64) Mazur, S.; Tanious, F. A.; Ding, D.; Kumar, A.; Boykin, D. W.; Simpson, I. J.; Neidle, S.; Wilson, W. D. *J. Mol. Biol.* **2000**, *300*, 321–337.
(65) Freyer, M. W.; Buscaglia, R.; Kaplan, K.; Cashman, D.; Hurley, L. H.; Lewis, E. A. *Biophys. J.* **2007**, *92*, 2007–2015.

JP7102676